Research Article | Vol. 27, No. 8 | 15 Apr 2019 | OPTICS EXPRESS 11312
Optics EXPRESS

Frequency modulated hybrid photonic crystal laser by thermal tuning

S. M. Butler,[1,2,*] A. P. Bakoz,[1,2] P. K. J. Singaravelu,[1,2] A. A. Liles,[3] B. O'Shaughnessy,[1,2] E. A. Viktorov,[4] L. O'Faolain[1,2,3] and S. P. Hegarty[1,2]

[1]*Centre for Advanced Photonics and Process Analysis, Cork Institute of Technology, Cork, Ireland*
[2]*Tyndall National Institute, Cork, Ireland*
[3]*Scottish Universities Physics Alliance (SUPA), School of Physics and Astronomy, St. Andrews, UK*
[4]*ITMO University, Saint Petersburg, Russia*
[*]*sharon.butler@mycit.ie*

Abstract: We demonstrate frequency modulation (FM) in an external cavity (EC) III-V/silicon laser, comprising a reflective semiconductor optical amplifier (RSOA) and a silicon nitride (SiN) waveguide vertically coupled to a 2D silicon photonic crystal (PhC) cavity. The PhC cavity acts as a tunable narrowband reflector giving wavelength selectivity. The FM was achieved by thermo-optical modulation of the reflector via a p-n junction. Single-mode operation was ensured by the short cavity length, overlapping only one longitudinal laser mode with the reflector. We investigate the effect of reflector modulation theoretically and experimentally and predict a substantial tracking of the resonator by the laser frequency with very small intensity modulation (IM).

1. Introduction

Frequency modulated (FM) lasers have been extensively researched due to their central importance in a wide range of applications such as bio-medical imaging [1], radar and sensing [2], and wide-band communications technology [3, 4]. Various realisations of FM semiconductor lasers have been reported with widely used monolithic solutions such as Distributed Bragg Reflector Super Structure Gratings (DBR-SSG) [3] and Distributed Feedback (DFB) lasers [5] which employ direct modulation of the laser injection current that modulates the laser intensity and frequency simultaneously. FM lasers for sensing applications are used with wavelength scanning absorption techniques and wide tuning with DFB lasers have been demonstrated for the application of gas sensing [6]. These devices offer a wide tuning range but the high fabrication complexity and increased power consumption during operation should be considered. With direct modulation, the simultaneous large intensity modulation (IM) combined with FM affects the sensitivity of the measurements over the frequency scan range. Numerous methods have been established to address this by extracting the frequency scan information such as second harmonic detection and subtraction techniques [7, 8]. The post processing of the signal information to account for the IM adds extra processing complexity therefore a pure FM laser can be more favourable for sensing applications as they eliminate the need for further calculations and processing of the frequency scan signal information.

In the optical communications field the Chirp Managed Laser (CML) [5] exploited FM to IM conversion to incorporate the effects of frequency chirp in Directly Modulated Lasers (DML) and use this for extended transmission distance. A pure FM laser is also desirable and Matsuo et al. [3] have demonstrated an extended transmission reach with a FM laser with constant output power with a SS-DBR multi-section laser. Modulation to the phase tuning section gave pure FM therefore the modulation speed was not limited by relaxation oscillations and then by optically

#354526 https://doi.org/10.1364/OE.27.011312
Journal © 2019 Received 4 Dec 2018; revised 12 Mar 2019; accepted 13 Mar 2019; published 9 Apr 2019

Optics EXPRESS

filtering the output light enabling conversion from FM to IM with a high extinction ratio.

Photonic integration on silicon is a promising solution for the mass production of complex photonic elements, due to features such as low-cost manufacture and energy consumption. Silicon has been the preferred material for photonic applications as it can be readily integrated with existing electronic circuit technologies and the fabrication process is well established. Previous research has demonstrated silicon-based resonant modulators in the form of a microdisk [9], racetrack resonator [10, 11] and microring resonator [12–14]. As silicon is not an ideal material for lasing, the use of III-V gain materials in a hybrid configuration has been explored as a solution. In this context, several configurations for an external cavity laser using silicon-based resonant reflectors have been previously demonstrated using silicon ring resonator devices [15–18]. This previous research has addressed the requirement for high extinction ratio needed for bandwidth in datacommunications by switching between on and off states at resonance with the lowest power consumption. Akiyama et al. [15] have achieved a large extinction ratio and Tanaka et al. [18] have exhibited an on-chip integrated device, by flip-chip bonding a III-V gain die to a silicon chip with a ring-resonator-based reflector.

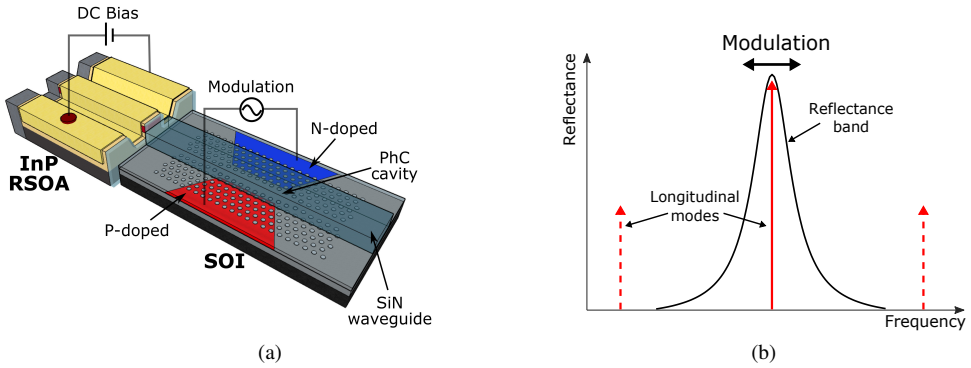

Fig. 1. (a) Laser configuration: III-V InP RSOA and silicon PhC cavity resonant reflector. Separate voltage to RSOA and modulating voltage to p-n junction at PhC cavity. (b) Reflectance band overlaps with one longitudinal mode. Modulation of lasing mode (laser FM) achieved by modulation of the reflectance band.

Here, we propose a hybrid laser with a III-V InP Reflective Semiconductor Optical Amplifier (RSOA) and a silicon Photonic Crystal (PhC) cavity resonant reflector (Fig. 1(a)), as per the configuration described in [19], where the resonant reflectance band of the PhC cavity overlaps with the longitudinal mode of the laser cavity that then lases (Fig. 1(b)). The use of a SiN waveguide gives considerable freedom in the choice of the mode size allowing a good match to be achieved with the RSOA waveguide. Additionally, the addition of the SiN layer gives the potential for integration of other devices, such multiplexer/demultiplexers. Previous research has demonstrated electro-optical modulation of the PhC cavity used in the Si-reflector using a p-n junction as a means of wavelength tuning the reflectance band [20] by carrier induced refractive index change. This work uses this approach and focuses on the thermo-optical effect in silicon as a means of achieving modulation of the lasing frequency. Modulation of the voltage passing through a doped p-n junction on the Si-reflector of the external cavity laser will change the refractive index which will tune the reflectance band and hence modulate the lasing frequency to satisfy the phase matching condition. PhC cavities have smaller modal area than a typical ring resonator and have a larger free spectral range (FSR) that results in less severe mode competition effects. The thermo-optical effect can achieve maximum speeds in the low MHz range which is sufficient for sensing applications. Thermal switching has been demonstrated by Beggs et al. [21] using a microheater on a PhC cavity/waveguide, while Akiyama et al. [15] and Lin et al. [16]

Optics EXPRESS

have also used the approach of an integrated microheater to tune the resonance wavelength of a ring resonator in a configuration that exhibits strong mode hopping. The work in this paper focuses on laser single mode FM with moderate tuning speed and small tuning range which also exhibits a low IM. This type of laser can be useful for applications where precise wavelength registration/high resolution is essential such as trace-gas detection. For gas detection techniques, a low IM over a frequency scan can be advantageous for identifying absorption features by eliminating the need for error correction of the signal or further calibration caused by IM.

This is the first time that this effect has been observed in a hybrid III-V/Silicon laser. Furthermore, by virtue of the small size of the photonic crystal cavity, some tuning can potentially be more efficient than the frequency tuning employed in III-V distributed feedback lasers.

2. Frequency modulated PhC laser theory

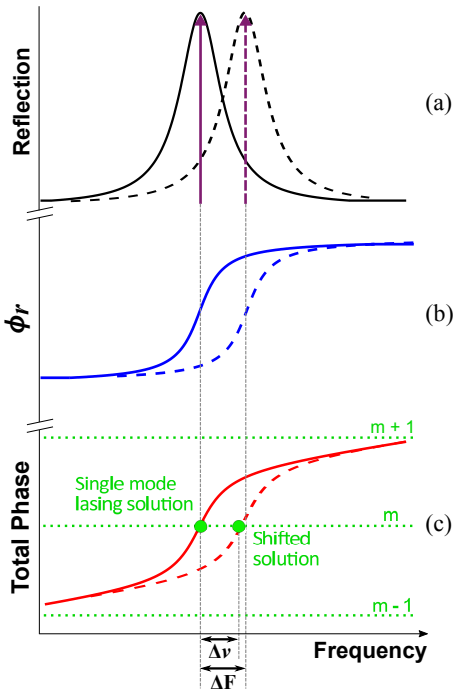

Fig. 2. (a) The reflection peak aligned with the longitudinal mode shifts by ΔF and (b) the reflection phase $\phi_r = arctan(2\pi\nu/\Gamma)$ occurs across reflection peak and shifts by same amount. (c) The total accumulated phase is the sum of the propagation phase $\phi_{prop} = 2\pi\nu T$ and the reflection phase. The single mode lasing solution exists at the intersection of the cavity mode m and the total accumulated phase. The solution shifts by $\Delta\nu$ and exists on the same cavity mode (green points).

As discussed in [19], the emitted wavelength of the PhC EC architecture is defined by the overlap of a longitudinal mode of the laser cavity with the reflection band of the PhC resonant reflector. In this paper we demonstrate FM of this configuration by tuning the resonance in the reflector via thermo-optical tuning of the p-n junction. [22–24] have measured experimentally the phase change over the reflection band for photonic crystals. Their results show the reflection phase ϕ_r shifts across the stop band of the reflective filter by $0 \leq \phi_r \leq \pi$. This is further illustrated for a PhC cavity in [25]. Assuming a Lorentzian shape for PhC cavity-based reflector (Fig. 2(a)),

Optics EXPRESS

close to the filter centre the reflection phase (Fig. 2(b)) is given by:

$$\phi_r = arctan\left(\frac{2\pi\nu}{\Gamma}\right) \approx \left(\frac{2\pi\nu}{\Gamma}\right) \tag{1}$$

where Γ is the reflection band width in radians, ν is the optical frequency and the linear approximation is valid close to the filter center, i.e. where the reflectivity is highest. The propagation phase ϕ_{prop} increases linearly with increasing frequency as given by $2\pi\nu T$, where T is the cavity roundtrip period therefore:

$$\phi_{prop} = \frac{2\pi\nu}{FSR} \tag{2}$$

where FSR is the Free Spectral Range. The sum of the propagation phase and the reflection phase is the total accumulated phase and the lasing solution is satisfied by:

$$\phi_{prop} + \phi_r = 2\pi m \tag{3}$$

where m is an integer. This is illustrated on Fig. 2(c) which shows the solution existing at the intersection of a laser cavity mode and the total accumulated phase, that lies within the reflection band. If the reflection band is tuned by ΔF, the phase at every frequency near the reflection band centre will change by:

$$\Delta\phi = -\Delta\mathrm{F}\left(\frac{2\pi}{\Gamma}\right) \tag{4}$$

To maintain the roundtrip phase condition the lasing mode shifts by $\Delta\nu$, leading to the following relation:

$$-\Delta\mathrm{F}\left(\frac{2\pi}{\Gamma}\right) + \Delta\nu\left(\frac{2\pi}{\Gamma}\right) + \Delta\nu\left(\frac{2\pi}{FSR}\right) = 0 \tag{5}$$

Re-arranging (5) gives the modal frequency shift needed to retain phase matching as (where Γ < FSR):

$$\Delta\nu = \Delta\mathrm{F}\left[\frac{1}{1+\frac{\Gamma}{FSR}}\right] \tag{6}$$

This linear approximation shows that the lasing frequency shift $\Delta\nu$ is less than the reflector shift ΔF (Fig. 2), and with a larger FSR to filter width ratio, the laser mode frequency follows the filter centre frequency more closely.

With this approximation, taking a value of a reflector width Γ = 15 GHz (linear, 94.3 in gigaradians per second) and FSR = 80 GHz, a lasing frequency shift $\Delta\nu$ of 5 GHz requires a reflector shift ΔF of 10.9 GHz. If our initial condition is that the starting mode-reflector detuning is zero i.e. 100% reflectivity, then for a lasing frequency shift of 5 GHz, this will result in a 0.7 dB reduction in the reflectivity which would require a modest 0.35 dB increase in the gain per pass to maintain lasing.

To examine the longitudinal mode tuning range as determined by the filter width and the FSR, we assume an allowed mode-to-filter detuning of one filter width ($|\Delta\mathrm{F} - \Delta\nu| \leq \Gamma/4\pi$) then from (6):

$$\left|\Delta\nu\left(1+\frac{\Gamma}{FSR}\right) - \Delta\nu\right| \leq \frac{\Gamma}{4\pi} \tag{7}$$

This gives then a maximum laser mode tuning range of:

$$\Delta\nu = \frac{FSR}{2\pi} \tag{8}$$

Optics EXPRESS

This result shows that the longitudinal mode tuning while remaining close to the filter centre depends only on the value of the FSR and it is independent of the width of the reflector, so for a larger FSR, a tuning of the lasing mode can be realised. Narrower values for Γ will lead to better mode-to-filter tracking, but the reflector half-width is proportionally smaller also and the two effects cancel (within the limits of the linear approximation).

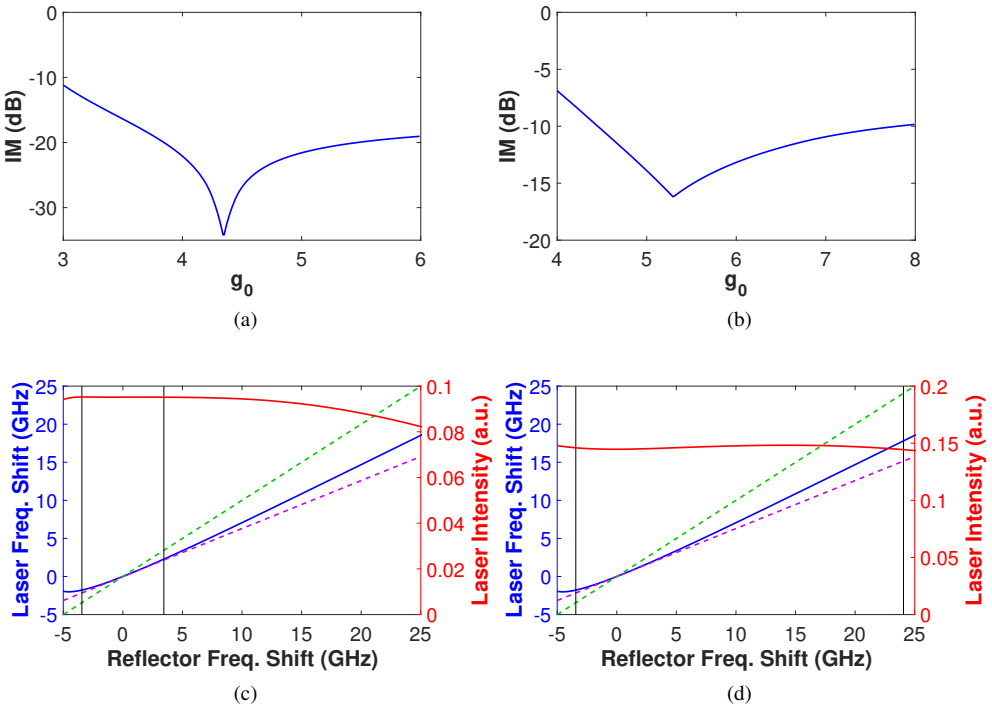

Fig. 3. Simulations of the IM vs. g_0 for modulation range of (a) 5 GHz and (b) 20 GHz. Laser output intensity (red) and laser frequency (blue) as a function of reflector shift for modulation range of (c) 5 GHz and (d) 20 GHz. The green dashed line indicates a perfect linear relationship between the laser and reflector63 frequency, the purple dashed line is the predicted linear relationship by Eq. (6). The solid black lines are the modulation range limits of 5 GHz and 20 GHz (6.88 GHz and 27.5 GHz for reflector). The parameters used for these simulations were: carrier recombination rate γ = 1 GHz, linear attenuation factor κ = 0.08, linewidth enhancement factor α = 3, roundtrip period T = 12.5 ps, reflector bandwidth Γ = 15 GHz, pump parameter g_0 = 3-8 varying for (a) and (b) then applied g_0 of 4.35 for (c) and 5.3 for (d).

To model the PhC laser numerically we use an adapted delay differential equation model for the electric field envelope and the saturable gain of the SOA, similar to that used to describe passively mode locked lasers in [26] but without the equation for saturable absorption. More details about this model may be found in [27]. The model applies SOA parameters and a Lorentzian shape filter which describes our laser system. We numerically explore the laser IM as a function of the DC biasing condition. These are expected to be related, as with fixed DC bias and a reduced output mirror reflectivity, the intra-cavity laser power will decrease (due to threshold increase), but at the same time a larger fraction of the internal power is transmitted as less power is being reflected back into the cavity. The SOA bias current is given by the pump parameter g_0.

Simulations were performed for varying values of g_0 and the IM over a given modulation range

was obtained. Figures 3(a) and 3(b) show the IM as a function of g_0. As explained in Section 1, a low IM or pure FM laser can be beneficial for communications or sensing applications therefore the lowest IM for a fixed g_0 is taken to be the optimal value. This value of g_0 was found to be 4.35 and 5.3 giving an IM of -34 dB and -16 dB for modulation ranges of 5 GHz and 20 GHz respectively.

In Figs. 3(c) and 3(d) the simulations were performed with the optimal g_0 applied. The laser intensity is indicated by the red line as a function of the reflector central frequency shift, which remains almost constant over the modulation range. Also shown is the relationship between the reflector central frequency shift and lasing frequency shift indicated by the blue line with zero detuning at frequency = 0 and it can be seen that as the reflector central frequency shifts, the laser frequency follows as predicted by the relationship in Eq. (6) and shown as the purple dashed line in Figs. 3(c) and 3(d). The green dashed line indicates a perfect linear relationship between the laser and reflector frequency. The vertical black lines are the modulation range limits of 5 GHz and 20 GHz.

3. Laser cavity

The EC laser was formed by the combination of an InP-based RSOA as the gain medium and a vertically coupled bus waveguide-PhC cavity-based narrowband reflector. Both elements were placed in close proximity through nano-positioning stages. Coupling was achieved by the butt-coupling of the gain medium waveguide to the SiN waveguide and thus the PhC cavity. The length of the RSOA waveguide was 400 µm which had a group index of 3.6 and the SiN waveguide length was 2240 µm, with a group index of 1.94 giving the total cavity optical length to be 5786 µm with a FSR of 25 GHz for the laser cavity.

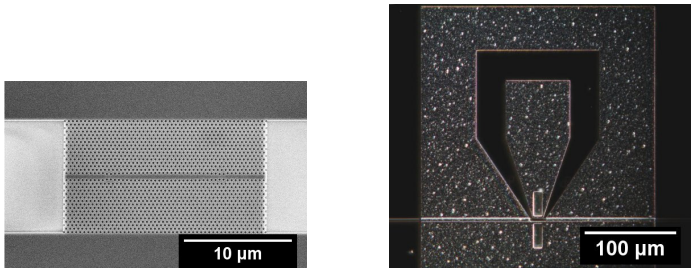

(a) (b)

Fig. 4. (a) SEM image of PhC cavity before p-n contact pads addition and (b) microscope image of PhC and p-n contact pads post fabrication.

The resonant reflectors are based on a vertically coupled PhC cavity waveguide system [28]. A low-refractive-index SiN waveguide is located vertically above a silicon PhC cavity. The two parts are separated by a thin oxide layer, which acts as a physical buffer and allows the evanescent exchange of light between the waveguide mode and the cavity mode [29]. For the experiments described here, a Dispersion Adapted (DA) PhC cavity design was chosen [30] as it offers high disorder tolerance and good mode overlap with the utilized low-index waveguides. The DA PhC cavity (Fig. 4(a)) was implemented on the 220 nm SOI platform by electron-beam lithography and Reactive Ion Etching (RIE). The height and width of the waveguide were 500 nm and 1 µm respectively, allowing low coupling losses to both the RSOA waveguide and the lensed fiber used to collect the output of the laser. Coupling losses from the RSOA and SiN waveguide were found to be 50% from Fimmwave simulation, and the losses are also shown for the same device interfaces in [31]. A ~170 nm thick layer of spin-on-glass (Accuglass by Honeywell) was used

Optics EXPRESS

as a buffer layer between the Si and SiN. Both facets of the reflector chip were coated with an anti-reflection layer (single layer MgF) to minimize back-reflections.

To create the p-n junction, four different levels of doping were used. The low doped p-n junction is designed to overlap with the DA cavity to achieve maximum electro-optic efficiency. The p-n junction is created by implantation of boron and phosphorous ions to realise the targeted doping concentration of 10^{16} cm^{-3}. Although the overlapped doping region increases the free-carrier losses, the measured loaded Q-factor of the cavity is 15,000, which is sufficient for our work. The p-n junction is designed 2 μm away from the center of the cavity. Rapid Thermal Annealing (RTA) is performed on the wafer for 60 seconds at 1000°C under N_2 environment to provide the maximum carrier activation.

To inject the free carriers into the p-n junction, the metal contacts (Fig. 4(b)) were formed by dry etching the vias holes through the oxide layer and then depositing aluminium contact pads. The heavy doped p-n junction helps to form an ohmic contact between the Si layer and Al pads, giving the low contact resistance (p = 240, n = 270 Ω/sq. sheet resistance). The estimated capacitance value for these devices is <1 pF, for a resistance of 0.5 kΩ, the RC constant is approximately 0.5 ns. This is not a limiting factor in this work as the thermal time constant will limit up to low MHz range.

Thermo-optic tuning of the PhC cavity resonance was caused by a local change in temperature - and thus the material refractive index - achieved by ohmic heating.

4. Experimental results

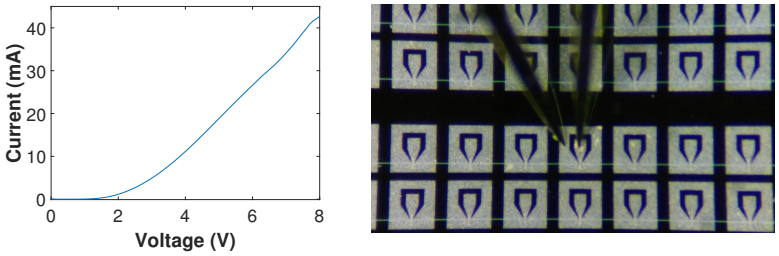

(a) (b)

Fig. 5. (a) IV curve for p-n junction. (b) Microscope image of needle probes applied to contact pads on sample.

The overall system temperature was maintained with Peltier element temperature controllers on both the RSOA and the PhC reflector chip. The IV curve in Fig. 5(a) was generated by applying voltage to the p-n contact pads of the silicon reflector using a voltage source and the needle probes as shown in Fig. 5(b) and measuring the current. The temperature rise generated from injection of carriers adjusted the temperature in the PhC cavity which in turn shifted the reflection peak of the reflective filter. A function generator was used to modulate the voltage to the contact pads and modulation of the lasing frequency was achieved.

Measurements were taken using the experimental setup shown in Fig. 6. The output of the laser was collected via a lensed fiber and passed through an isolator (ISO) then to a 1x2 splitter with one path to a channel of the oscilloscope (OSC) to capture the output intensity and the other path was passed through a 3x3 splitter and mixed with tunable laser source (TLS). A beating signal was generated by setting the TLS output close to the lasing wavelength and mixing these two signals. The beating frequency was observed on a 33 GHz bandwidth oscilloscope making it possible to capture the fast frequency dynamics of the laser and thus observing the laser frequency

Optics EXPRESS

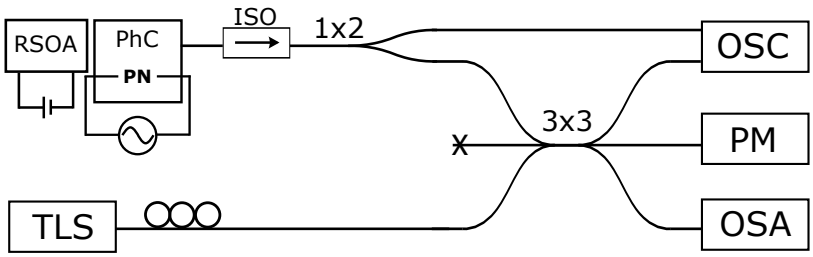

Fig. 6. Experimental Setup.

modulation generated by the modulation of the PhC temperature. A power meter (PM) and optical spectrum analyser (OSA) measured the output power and recorded the optical spectrum.

Figure 7(a) shows single mode operation was achieved with a lasing wavelength of ~1540.5 nm and a SMSR (Side Mode Suppression Ratio) of ~30 dB at a pumping current of 50 mA. The LI curve shows a threshold value of approx. 15 mA and the kink at 30 mA indicates a mode hop. There is stable single mode operation from 30 - 90 mA. This laser had a typical linewidth value of 4 MHz. We also observe the gain ripple from the RSOA in the optical spectrum, nonetheless the SMSR is 30 dB. The distance between peaks is ~1 nm. The FSR of the PhC is larger than this and can be determined from the transmission spectrum, similar to the devices used in [20], where the PhC cavity FSR is ~8 nm.

With the gain biased at 50 mA and on applying DC voltage to the p-n junction, a shift of the single mode lasing peak was observed. Using the heterodyne measurement with the TLS to capture the beating frequency, applying 4.2 - 4.7 V stepped DC voltage gave a frequency shift of the lasing peak of ~6.5 GHz for an applied heating power of 20 mW (Fig. 7(b)).

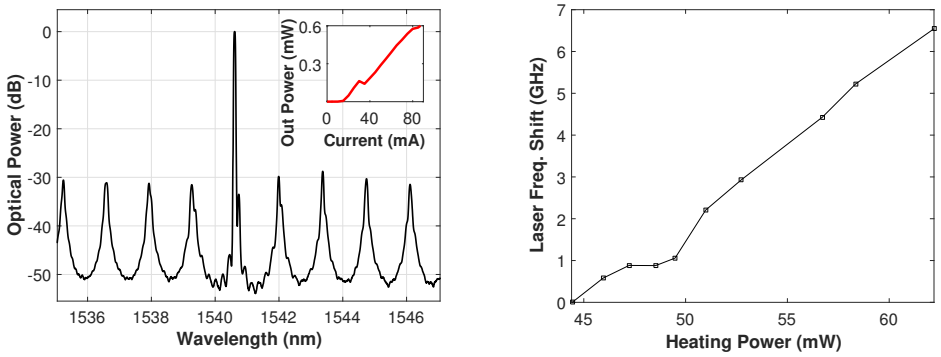

(a) (b)

Fig. 7. (a) Single mode operation at ~1540.5 nm, SMSR ~30 dB at a pumping current of 50 mA. Inset: Measured LI curve, threshold ~15 mA. (b) Frequency shift of lasing peak as a function of heating power by heterodyne measurement with TLS.

The heat is dissipated in the highly thermally conductive silicon layer, which is thermally isolated from the SiN waveguide. Coupled with the low thermo-optic coefficient of SiN, any effects of the p-n junction on the optical length of the silicon nitride is negligible. To observe the frequency modulation and intensity modulation simultaneously, a triangular wave signal of 2.7 - 4 V at 10 kHz was applied to the p-n junction (Fig. 8(a)). The laser output intensity modulation showed to follow the frequency modulation and had a value of -8.7 dB (Fig. 8(b)). This value

Optics EXPRESS

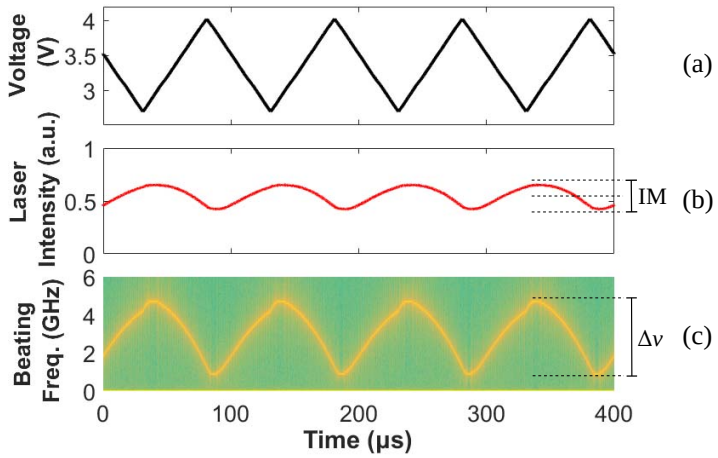

Fig. 8. (a) Driving signal input to p-n junction, (b) laser output intensity with IM of -8.7 dB and (c) beating frequency showing FM of the laser giving a frequency shift $\Delta\nu$ of ~4 GHz.

could be further reduced by optimising the pumping current as described in the simulations in Section 2. This IM value is not as low as the simulation results due to idealised simulation parameters used which do not account for non-ideal experimental conditions. The frequency shift $\Delta\nu$ was ~4 GHz (Fig. 8(c)) for this drive signal range. The shape of the frequency modulation is distorted to the triangular waveform input which is to be expected as the reflector shift and frequency shift do not have the perfect linear relationship shown in the simulations. Also, the curvature in the FM shape could be explained by the effects of two photon absorption and free carrier absorption on the PhC cavity temperature and resonance wavelength [19].

5. Conclusion

We have presented a FM PhC laser by means of the thermo-optic effect in silicon. It can be seen in this work that the resonance wavelength shift in the laser cavity can be achieved by local heating of the PhC cavity. The laser output power was lower than expected for similar configurations due to the coupling losses between the RSOA, waveguide and lensed fiber caused mainly by alignment stability issues, this also had an effect on the required power for the resonance shift. These values can be improved upon with better coupling efficiency between the waveguides by the application of better anti-reflection coatings and angled waveguides on the facets to minimise parasitic reflections in the laser cavity. Improvements in heating efficiency can be achieved by trenching and undercutting around PhC cavity for thermal isolation and simulations show an improvement of three times less the amount of required heating power for the same shift using the undercutting approach in [10, 19].

Experimentally we have shown that the laser shift does indeed track the filter shift although weakly in these results. The weak tracking is due to the wide reflective filter width for these particular devices used in these experiments. Further optimisation of the fabrication process can reduce the reflective filter width leading to better tracking of the laser as shown in the calculations above.

We have demonstrated an applied heating power of 20 mW to achieve the DC frequency shift of ~6.5 GHz. Theoretically the IM value is lower than what was achieved experimentally as not all the simulation parameters account for experimental conditions such as imperfect anti-reflective coatings on RSOA and PhC chip facets. Nevertheless both the theoretical and

Optics EXPRESS

experimental results show a very small IM which has the potential to realise a pure FM laser that can find applications in wavelength scanning absorption techniques such as FM spectroscopy and trace-gas detection where a narrow tuning range is sufficient and a high sensitivity FM is required. The p-n junction was operated in forward bias at low modulation speeds to study the thermo-optic effect. With these devices, the p-n junction can also be operated in reverse bias for carrier depletion which has the potential to achieve GHz speeds which can find applications in the optical communications field.

Funding

Science Foundation Ireland (SFI 12/RC/2276, SFI 16/ERCS/3838); Engineering and Physical Sciences Research Council (EPSRC) (doctoral grant EP/L505079/1); H2020 European Research Council (ERC) (starting grant 337508); Scottish Enterprise; Cork Institute of Technology (CIT) (Rísam); Irish Government's Programme for Research in Third Level Institutions, Cycle 5, Strand 1a (CREATE).

References

1. Z. D. Taylor, R. S. Singh, D. B. Bennett, P. Tewari, C. P. Kealey, N. Bajwa, M. O. Culjat, A. Stojadinovic, H. Lee, J. Hubschman, E. R. Brown, and W. S. Grundfest, "THz medical imaging: in vivo hydration sensing," IEEE Trans. Terahertz Sci. Technol. **1**, 201–219 (2011).
2. J. Lin, C. Lu, H. . Chuang, F. . Kuo, J. Shi, C. Huang, and C. Pan, "Photonic generation and detection of w-band chirped millimeter-wave pulses for radar," IEEE Photonics Technol. Lett. **24**, 1437–1439 (2012).
3. S. Matsuo, T. Kakitsuka, T. Segawa, N. Fujiwara, Y. Shibata, H. Oohashi, H. Yasaka, and H. Suzuki, "Extended transmission reach using optical filtering of frequency-modulated widely tunable SSG-DBR laser," IEEE Photonics Technol. Lett. **20**, 294–296 (2008).
4. P. A. Morton, G. E. Shtengel, L. D. Tzeng, R. D. Yadvish, T. Tanbun-Ek, and R. A. Logan, "38.5 km error free transmission at 10 Gbit/s in standard fibre using a low chirp, spectrally filtered, directly modulated 1.55 μm DFB laser," Electron. Lett. **33**, 310–311 (1997).
5. Y. Matsui, D. Mahgerefteh, X. Zheng, C. Liao, Z. F. Fan, K. McCallion, and P. Tayebati, "Chirp-managed directly modulated laser (CML)," IEEE Photonics Technol. Lett. **18**, 385–387 (2006).
6. V. Weldon, J. O'Gorman, P. Phelan, J. Hegarty, and T. Tanbun-Ek, "H2S and CO2 gas sensing using DFB laser diodes emitting at 1.57 μm," Sens. Actuators, B **29**, 101–107 (1995).
7. S. Schilt, L. Thévenaz, and P. Robert, "Wavelength modulation spectroscopy: combined frequency and intensity laser modulation," Appl. Opt. **42**, 6728–6738 (2003).
8. H. Li, G. B. Rieker, X. Liu, J. B. Jeffries, and R. K. Hanson, "Extension of wavelength-modulation spectroscopy to large modulation depth for diode laser absorption measurements in high-pressure gases," Appl. Opt. **45**, 1052–1061 (2006).
9. M. R. Watts, W. A. Zortman, D. C. Trotter, R. W. Young, and A. L. Lentine, "Vertical junction silicon microdisk modulators and switches," Opt. Express **19**, 21989–22003 (2011).
10. P. Dong, W. Qian, H. Liang, R. Shafiiha, D. Feng, G. Li, J. E. Cunningham, A. V. Krishnamoorthy, and M. Asghari, "Thermally tunable silicon racetrack resonators with ultralow tuning power," Opt. Express **18**, 20298–20304 (2010).
11. J.-B. You, M. Park, J.-W. Park, and G. Kim, "12.5 Gbps optical modulation of silicon racetrack resonator based on carrier-depletion in asymmetric p-n diode," Opt. Express **16**, 18340–18344 (2008).
12. F. Gardes, A. Brimont, P. Sanchis, G. Rasigade, D. Marris-Morini, L. O'Faolain, F. Dong, J. Fedeli, P. Dumon, L. Vivien, T. Krauss, G. Reed, and J. Martí, "High-speed modulation of a compact silicon ring resonator based on a reverse-biased pn diode," Opt. Express **17**, 21986–21991 (2009).
13. Q. Xu, S. Manipatruni, B. Schmidt, J. Shakya, and M. Lipson, "12.5 Gbit/s carrier-injection-based silicon micro-ring silicon modulators," Opt. Express **15**, 430–436 (2007).
14. P. Dong, W. Qian, H. Liang, R. Shafiiha, N.-N. Feng, D. Feng, X. Zheng, A. V. Krishnamoorthy, and M. Asghari, "Low power and compact reconfigurable multiplexing devices based on silicon microring resonators," Opt. Express **18**, 9852–9858 (2010).
15. T. Akiyama, S. Tanaka, T. Kurahashi, H. Ebe, and S. Sekiguchi, "A novel transmitter leveraging high-speed ultralow-power modulation of a Si microring modulator by eliminating tuning power," in *2016 Optical Fiber Communications Conference and Exhibition (OFC),* (Optical Society of America, 2016), pp. 1–3.
16. S. Lin, S. S. Djordjevic, J. E. Cunningham, I. Shubin, Y. Luo, J. Yao, G. Li, H. Thacker, J.-H. Lee, K. Raj, X. Zheng, and A. V. Krishnamoorthy, "Vertical-coupled high-efficiency tunable III-V- CMOS SOI hybrid external-cavity laser," Opt. Express **21**, 32425–32431 (2013).
17. T. Chu, N. Fujioka, and M. Ishizaka, "Compact, lower-power-consumption wavelength tunable laser fabricated with silicon photonic wire waveguide micro-ring resonators," Opt. Express **17**, 14063–14068 (2009).

Optics EXPRESS

18. S. Tanaka, S.-H. Jeong, S. Sekiguchi, T. Kurahashi, Y. Tanaka, and K. Morito, "High-output-power, single-wavelength silicon hybrid laser using precise flip-chip bonding technology," Opt. Express **20**, 28057–28069 (2012).
19. A. Bakoz, A. Liles, A. Gonzalez-Fernandez, T. Habruseva, C. Hu, E. A. Viktorov, S. P. Hegarty, and L. O'Faolain, "Wavelength stability in a hybrid photonic crystal laser through controlled nonlinear absorptive heating in the reflector," Light. Sci. Appl. **7**, 39 (2018).
20. K. Debnath, L. O'Faolain, F. Y. Gardes, A. G. Steffan, G. T. Reed, and T. F. Krauss, "Cascaded modulator architecture for WDM applications," Opt. Express **20**, 27420–27428 (2012).
21. D. M. Beggs, T. P. White, L. Cairns, L. O'Faolain, and T. F. Krauss, "Ultrashort photonic crystal optical switch actuated by a microheater," IEEE Photonics Technol. Lett. **21**, 24–26 (2009).
22. M. Golosovsky, Y. Neve-Oz, D. Davidov, and A. Frenkel, "Phase shift on reflection from metallodielectric photonic bandgap materials," Phys. Rev. B **70**, 115105 (2004).
23. E. Ozbay and B. Temelkuran, "Reflection properties and defect formation in photonic crystals," Appl. Phys. Lett. **69**, 743–745 (1996).
24. E. Istrate and E. H. Sargent, "Measurement of the phase shift upon reflection from photonic crystals," Appl. Phys. Lett. **86**, 151112 (2005).
25. J. Mork, Y. Chen, and M. Heuck, "Photonic crystal fano laser: Terahertz modulation and ultrashort pulse generation," Phys. Rev. Lett. **113**, 163901 (2014).
26. A. Vladimirov and D. Turaev, "Model for passive mode locking in semiconductor lasers," Phys. Rev. A **72**, 033808 (2005).
27. S. Slepneva, B. Kelleher, B. O'Shaughnessy, S. P. Hegarty, A. Vladimirov, and G. Huyet, "Dynamics of Fourier domain mode-locked lasers," Opt. Express **21**, 19240–19251 (2013).
28. A. A. Liles, K. Debnath, and L. O'Faolain, "Lithographic wavelength control of an external cavity laser with a silicon photonic crystal cavity-based resonant reflector," Opt. Lett. **41**, 894–897 (2016).
29. K. Debnath, K. Welna, M. Ferrera, K. Deasy, D. G. Lidzey, and L. O'Faolain, "Highly efficient optical filter based on vertically coupled photonic crystal cavity and bus waveguide," Opt. Lett. **38**, 154–156 (2013).
30. K. Welna, S. L. Portalupi, M. Galli, L. O'Faolain, and T. F. Krauss, "Novel dispersion-adapted photonic crystal cavity with improved disorder stability," IEEE J. Quantum Electron. **48**, 1177–1183 (2012).
31. S. Iadanza, A. P. Bakoz, P. K. J. Singaravelu, D. Panettieri, S. A. Schulz, G. C. R. Devarapu, S. Guerber, C. Baudot, F. Boeuf, S. P. Hegarty, and L. O'Faolain, "Thermally stable hybrid cavity laser based on silicon nitride gratings," Appl. Opt. **57**, E218–E223 (2018).